Deciphering Degassing and Source Effects in Cl Isotopes in Melt Inclusions: The Possible Role of Amphibole in the Magma Source of Stromboli (Aeolian Island Arc)

Anne-Sophie Bouvier[1]*, Estelle F. Rose-Koga[2] and Alexis Chapuis[2]

[1]*Institut des Sciences de La Terre, Université de Lausanne, Lausanne, Switzerland, [2]Université Clermont-Auvergne, CNRS, IRD, OPGC, Laboratoire Magmas et Volcans, Clermont-Ferrand, France*

Chlorine isotopes have emerged as a new geochemical tool over the past 15 years. Most of the data consist of bulk rock data, with a minority carried out *in situ* on melt inclusions using secondary ion mass spectrometry. More data are necessary to understand the relationship between $\delta^{37}Cl$ measured in melt inclusions and that in bulk rocks from the same volcanic center. Here we have analyzed a suite of melt inclusions entrapped in olivine Fo_{63-85}, as well as some from clinopyroxene crystals, from a single hand-sample from the Vancori unit of Stromboli, Aeolian Islands. The 27 selected melt inclusions have major element compositions ranging from high potassium alkali basalt to evolved shoshonite. Their $\delta^{37}Cl$ vary from $-2.6 \pm 0.1‰$ to $+1.2 \pm 0.2‰$, a far larger range than for Stromboli bulk rocks. In this dataset, the $\delta^{37}Cl$ variation in melt inclusions is not related to Cl degassing, or to fractional crystallization. Instead, correlations between $\delta^{37}Cl$ and S/Cl, K_2O and trace element ratios suggest mixing of two Cl endmembers with distinct $\delta^{37}Cl$ signatures. A first endmember is characterized by high potassium alkali basalt compositions, high Ba/La (~28), high S/Cl, and high $\delta^{37}Cl$ (>1‰), confirming the influence in the mantle source of an aqueous fluid and providing a new constraint on its composition: that it derives from the breakdown of amphibole. The second endmember has a more evolved composition, high La/Yb, low S/Cl, and low $\delta^{37}Cl$ (<−2‰), identifying the influence of a solute-rich component derived from subducted sediments. The $\delta^{37}Cl$ data thus help refine the two sources initially identified from bulk rock studies and $\delta^{37}Cl$ proves to be a potential tracer for amphibole.

Keywords: SIMS, Cl isotopes, subduction, Aeolian Island arc, arc magmas, slab contribution

INTRODUCTION

Chlorine is one of the most abundant volatile elements, along with water, carbon, and sulfur, and is the most abundant halogen element. Its concentration in arc magmas can reach up to 7,500 µg/g (e.g., Aiuppa et al., 2009 for a review), whereas it is usually less than 100 µg/g in unaltered MORB samples (e.g., Jambon et al., 1995). Some unaltered MORB samples can however exhibit high Cl contents (up to > 100 µg/g) associated with high Cl/K due to assimilation of altered material (e.g., Marschall et al., 2017). Chlorine has two stable isotopes, which fractionate at low temperatures

(Schauble et al., 2003). Chlorine isotopes have been used to track the deep Cl cycle as well as the behavior of Cl during degassing (e.g., Barnes et al., 2008; Barnes et al., 2009; Sharp et al., 2010; Chiaradia et al., 2014; Bouvier et al., 2019). As summarized by Barnes and Sharp (2017), terrestrial whole rocks span a relatively large range in terms of $\delta^{37}Cl$, ranging from −3.7 to +3.0‰. The most negative values are usually attributed to sediments or sediments influenced by magma genesis, whereas the most positive values might reflect the influence of amphibole (Barnes and Cisneros, 2012). Indeed, based on theoretical and experimental results, amphibole can be slightly enriched in ^{37}Cl compared to co-existing fluids (Schauble et al., 2003; Cisneros, 2013). Barnes and Sharp (2017) pointed out that despite the theoretical fractionation at high temperature (700°C) between amphibole and a fluid at equilibrium, there might be another process, such as kinetic fractionation, shifting the $\delta^{37}Cl$ to the highest measured values (up to 1.8‰). During degassing, Cl isotopes do not usually fractionate. However, Sharp et al. (2010) demonstrated that while Cl isotope fractionation between silicate melt and gaseous HCl is limited (<0.6‰ at 500°C), the Cl isotopes could significantly fractionate toward strongly positive values at near surface pressures, due to interaction between gaseous HCl and liquid phases. Also, Fortin et al. (2017) showed that Cl isotopes could be largely fractionated during diffusion (up to 5‰), ^{35}Cl moving faster in the vapor phases, leading to a progressively ^{37}Cl-enriched degassed melt phase. Recently, $\delta^{37}Cl$ has been measured in situ in melt inclusions (Bouvier et al., accepted; Layne et al., 2009; Manzini et al., 2017; Bouvier et al., 2019). These melt inclusions preserve the least degassed Cl compositions compared to bulk rock, and the diffusion of Cl out of the melt inclusions is limited due to the large ionic radius of Cl⁻ (Le Voyer et al., 2014).

There are several factors that make Stromboli a good study-volcano for deciphering the different slab inputs into the mantle source of the magma. In addition to the high diversity of geochemical compositions of the erupted products (e.g., Francalanci et al., 1988; Francalanci et al., 1989; Francalanci et al., 2007) and its persistent activity, the subducting Ionian plate (slab) has a high-angle dip (about 70°), and this slab is reported to be almost entirely recycled into the mantle (e.g., Gvirtzman and Nur, 1999; Meletti et al., 2000; Gvirtzman and Nur, 2001; Pontevivo and Panza, 2006). Bulk rock studies of lavas from Stromboli reported that the geochemical characteristics of the erupted magmas revealed a contribution from both altered oceanic basalt and sediments from the subducted slab (e.g., Francalanci et al., 2007). Stromboli melt inclusion studies based on major and trace elements and isotopes have confirmed the contribution of these two slab components (e.g., Rose-Koga et al., 2012), and in some cases have added constraints as to the nature of the contribution (e.g., Schiavi et al., 2012). More recent studies, using the relatively new chlorine isotope systematics, have shown that Stromboli melt inclusions have lower $\delta^{37}Cl$ (−3.2 to −1.4‰, n = 5; Manzini et al., 2017) compared to bulk rocks from the same island (−1.0 to +0.7‰, n = 7; Liotta et al., 2017). Bouvier et al. (2019) suggested that melt inclusions preserve the $\delta^{37}Cl$ signature of an undegassed melt, while the bulk rocks might have been affected by fractionation

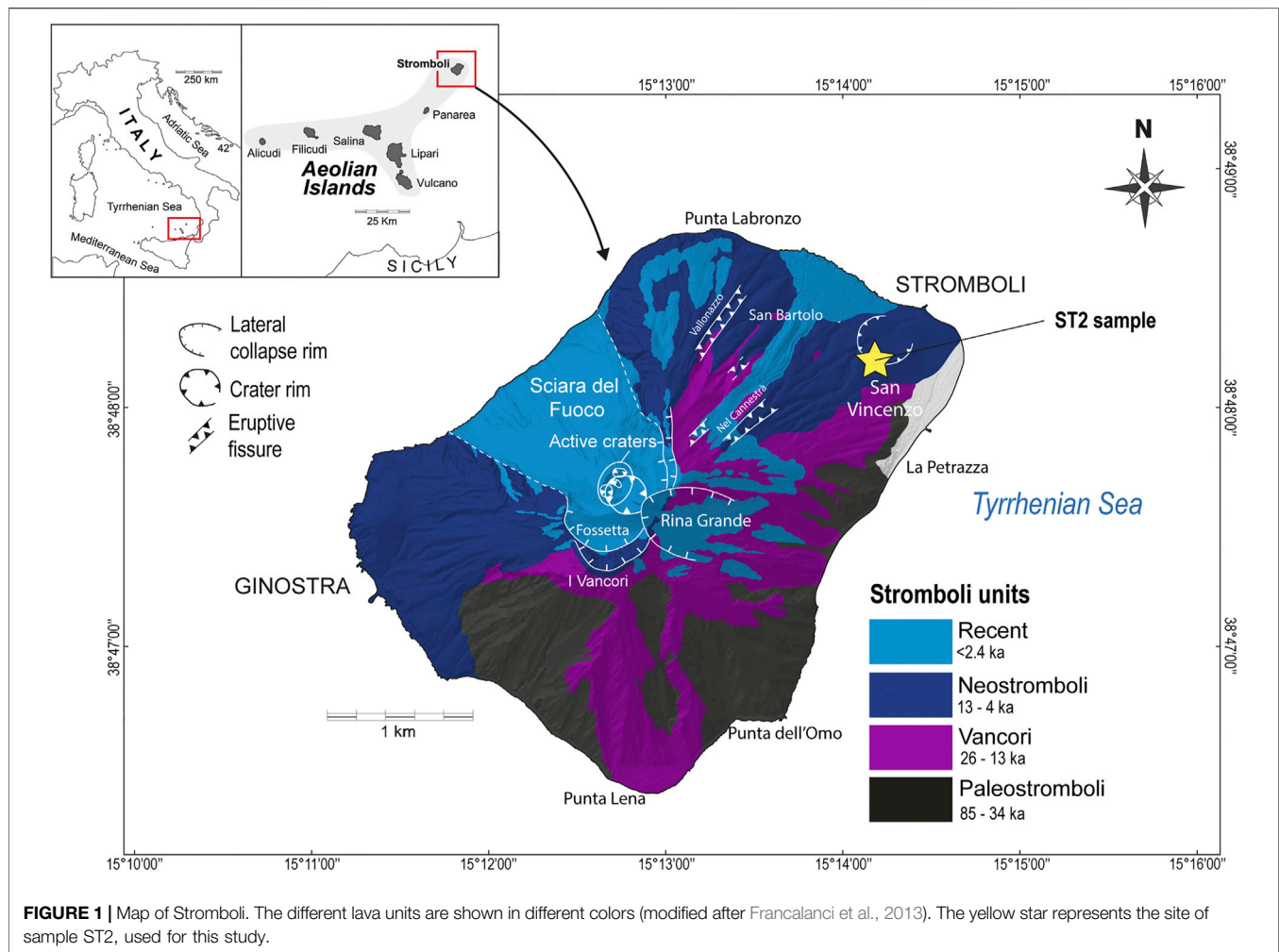during shallow degassing. This was supported by gas measurements showing negative $\delta^{37}Cl$ values (down to −2.2‰; Liotta et al., 2017). In order to test this hypothesis here, we measured $\delta^{37}Cl$ in melt inclusions from one single hand-sample from Stromboli (Vancori unit 26,000–13,000 years; e.g., Francalanci et al., 2013), in olivines covering a wide range of forsterite (Fo) contents and in a few pyroxenes. Thus, the melt inclusions we analyzed represent the progressive chemical change of the magma (by crystallization and degassing) in which they crystallized, and we can identify (and quantify) the magmatic processes that cause the $\delta^{37}Cl$ variations.

We found that the melt inclusions recorded a greater variation in $\delta^{37}Cl$ than previously reported by Manzini et al. (2017), almost as large as that of the $\delta^{37}Cl$ measured in Stromboli gas samples, and far greater than that reported for bulk rocks from Stromboli (Liotta et al., 2017). Combined with major and trace elements, our results confirm that Cl isotopes are not significantly fractionated during magma crystallization or during magma degassing. The $\delta^{37}Cl$ results suggest that the Cl addition beneath Stromboli originates from the subducted sediments and that $\delta^{37}Cl$ is a tracer of amphibole breakdown. $\delta^{37}Cl$ could prove to be a useful geochemical tool to trace the potentially widespread "cryptic amphibole fractionation" which occurs during the differentiation of arc magmas (Davidson et al., 2007).

GEOLOGICAL CONTEXT

Stromboli is located at the eastern end of the Aeolian arc (southern Italy), generated by the active subduction of the African plate beneath the European plate (e.g., Barberi et al., 1974; Gasparini et al., 1982; Ellam et al., 1989). Geophysical data indicate the presence of a slab (about 200 km wide) dipping at a high angle of ~50–70° to the northwest below the Aeolian arc. Volcanic activity on Stromboli can be divided into four main periods over the last 100 ka (e.g., Francalanci et al., 2013). These eruptions have led to a great diversity of volcanic products which can be classified into four series based on their SiO_2 and K_2O content: calc-alkaline, high-potassium calco alkaline, shoshonitic, and potassic (e.g., Francalanci et al., 2013).

The increase in K_2O from calc-alkaline to shoshonitic to potassic magmas is associated with a decrease in $^{143}Nd/^{144}Nd$ and an increase in $^{87}Sr/^{86}Sr$ ratios (e.g., Francalanci et al., 2007). Similarly, incompatible trace elements tend to increase from calc-alkaline to potassic (Francalanci et al., 2007). This wide variability of geochemical signatures encountered in the magmas of Stromboli is mostly acquired in the mantle wedge, with limited assimilation of continental crust (e.g., Francalanci et al., 1988; Ellam et al., 1989; Francalanci et al., 1989; Ellam and Harmon, 1990; Francalanci et al., 1993; De Astis et al., 2000; Francalanci et al., 2004; Francalanci et al., 2007; Tommasini et al., 2007). The processes responsible for this geochemical heterogeneity of the mantle wedge beneath Stromboli are attributed to complex melting and/or dehydration mechanisms in the Ionian slab (e.g., Schiavi et al., 2012).

FIGURE 1 | Map of Stromboli. The different lava units are shown in different colors (modified after Francalanci et al., 2013). The yellow star represents the site of sample ST2, used for this study.

The plumbing system of Stromboli is thought to have at least two (e.g., Vaggelli et al., 2003) or three (Francalanci et al., 2005) melt reservoirs. Present day activity is characterized by persistent moderate explosions (Strombolian activity), emitting highly porphyric (HP) scoriae and lavas, whereas during paroxysmal eruptions pumices with low phenocryst contents (LP) are emitted (Francalanci et al., 2004). LP magmas are suggested to originate from a deep reservoir (~10–11 km, e.g., Bertagnini et al., 2003; Vaggelli et al., 2003; Pino et al., 2011), with HP melts deriving from LP through degassing, crystallization, and mixing in a shallower reservoir (~1–3 km; e.g., Vaggelli et al., 2003; Burton et al., 2007; Métrich et al., 2010).

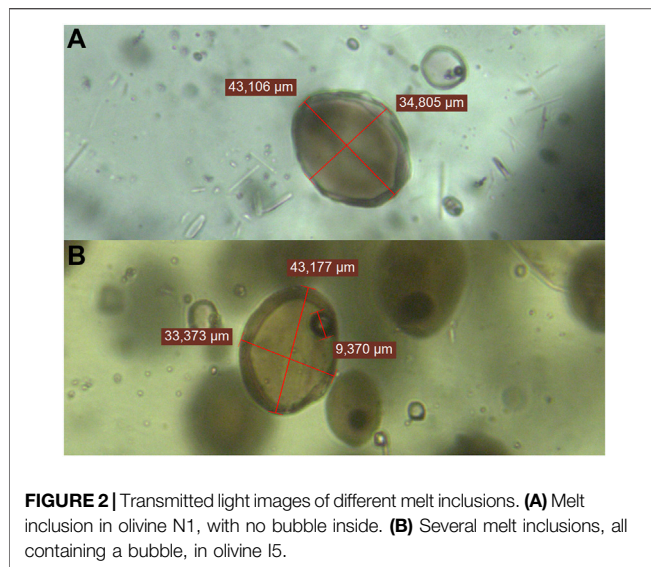## MATERIAL AND METHODS

Material
The sample studied is ST2, the same one that was used for four out of five of Manzini et al. (2017)'s melt inclusion data. This sample comes from a basaltic lapilli deposit of the Vancori unit (**Figure 1**). Olivine grains and a few pyroxene grains were

handpicked to select crystals that had an exposed surface of glassy melt inclusion, of more than 30 µm in size and free of cracks. Almost half of the melt inclusions contained a shrinkage bubble (**Figure 2**).

Methods
Electron Microprobe
Major elements in melt inclusions and olivines were measured by electron microprobe using a Cameca SXFive-TACTIS at the Laboratoire Magmas et Volcans (Clermont-Ferrand, France). Melt inclusions were analyzed using a defocused 10 µm beam, at 8 nA and 15 kV, whereas olivine grains were measured with a focused beam at 15 nA and 15kV, following the procedure described in Rose-Koga et al. (2021). Sulfur and Cl were also determined in melt inclusions using a 10-µm beam at 40 nA, 15 kV. Glass VG2 (Jarosewich et al., 1980) was also measured during the session to check the accuracy of the measurements. The errors on the measurement for each element are given in 1σ for host crystals and 3σ for melt inclusions: typically <1% SiO_2, Al_2O_3, FeO, MgO, CaO, K_2O, <4% TiO_2, <2% Na_2O, <20% MnO, P_2O_5, and <10% Cl, S. The analytical conditions are summarized in the **Supplementary Table S1**.

FIGURE 2 | Transmitted light images of different melt inclusions. (A) Melt inclusion in olivine N1, with no bubble inside. (B) Several melt inclusions, all containing a bubble, in olivine I5.

FIGURE 3 | Instrumental mass fractionation plotted against the equation defined by Manzini et al. (2017). The different reference materials used are the same as in Manzini et al. (2017) and all have more than 1,000 µg/g Cl.
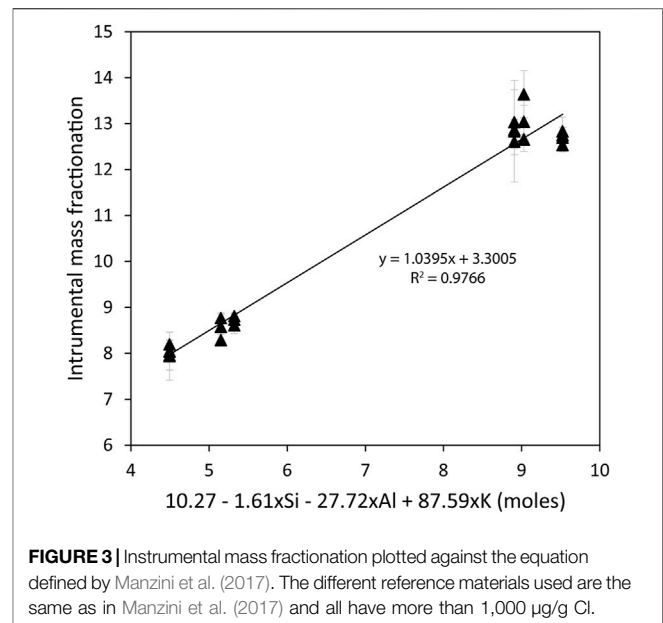
SIMS

Chlorine isotopes were measured in melt inclusions using a CAMECA 1280HR at the University of Lausanne, following the protocol of Manzini et al. (2017). In brief, a Cs^+ source was used to bombard the sample surface with an acceleration voltage of 10 kV and a primary intensity of 3 nA. An electron gun was used to compensate the build-up of charge on the sample surface. $^{35}Cl^-$ and $^{37}Cl^-$ were collected simultaneously in two faraday cups equipped with $10^{11}\Omega$ resistors. Each measurement started with 150 s pre-sputtering using a 25-µm raster and automated centering in field and contrast apertures, followed by 40 cycles of 4 s of acquisition. This led to an average measurement uncertainty of ~0.15‰ (2 standard errors, 2SE). Mass was stabilized using nuclear magnetic resonance. Calibration of the mass instrumental fractionation was done using Manzini et al. (2017) reference material (**Figure 3**). Reproducibility of the standards was greater than 0.35‰ (2 standard deviations, 2SD), except for the less homogeneous reference material RMR (Godon et al., 2004; Manzini et al., 2017) which usually reproduced at 1‰ (2SD). Reference material UNIL-B4 and UNIL-B6 were also on ST2 mounts. Repeated measurements of these reference materials during the 6-h session showed a reproducibility of 0.27 and 0.20‰ (2SD), respectively (see **Supplementary Material S2**). Accuracy of the measurements, defined here as the deviation of the reference materials from the calibration line, is 0.26‰ on average, but could reach up to 0.5‰ for PR2 reference material (Godon et al., 2004; Manzini et al., 2017).

LA-ICP-MS

Most melt inclusions were also analyzed for trace elements. A few were either too thin or too small to extract reliable LA-ICP-MS data.

Trace element abundances of the melt inclusions were analyzed by laser ablation-inductively coupled plasma mass spectrometry (LA-ICP-MS) at the Laboratoire Magmas et Volcans, Clermont-Ferrand, France using a 193 nm Excimer Resonetics M-50E laser with an Agilent 7500 ICP–MS. Analysis followed routine in-house procedures outlined in previous studies (e.g., Le Voyer et al., 2010; Rose-Koga et al., 2012). Briefly, a pulse energy of about 5 mJ was used with a spot diameter of between 20 and 33 µm (depending on melt inclusion size), and a laser pulse frequency of 2 Hz, to keep a fluence at sample surface of about 2.70 J/cm^{-2}. The following masses were analyzed for the target elements: ^6Li, ^7Li, ^{43}Ca, ^{44}Ca, ^{45}Sc, ^{47}Ti, ^{51}V, ^{59}Co, ^{60}Ni, ^{63}Cu, ^{85}Rb, ^{88}Sr, ^{89}Y, ^{90}Zr, ^{93}Nb, ^{137}Ba, ^{139}La, ^{140}Ce, ^{141}Pr, ^{146}Nd, ^{147}Sm, ^{153}Eu, ^{157}Gd, ^{163}Dy, ^{166}Er, ^{172}Yb, ^{175}Lu, ^{178}Hf, ^{181}Ta, ^{208}Pb, ^{232}Th, ^{238}U. The background was measured for about 30 s before ablation and analysis time was approximately 100 s. This technique uses CaO (measured by electron microprobe) as an internal standard during data reduction with the GLITTER software (www.es.mq.edu.au/GEMOC). Systematic analysis of two glass reference materials (BCR2-G and NIST 612; see **Supplementary Material**) before, after, and during the session were used to determine the reproducibility and accuracy of the analysis. The average 1σ error of the mean on the samples was less than 10% for all trace elements, except for Lu (<20%) and B (<40%).

RESULTS

Olivine hosts have a forsterite content (Fo = 100 × Mg/(Fe + Mg)) ranging from 66.8 to 84.6. Melt inclusions hosted in these olivines were corrected for post-entrapment crystallization using Petrolog software (Danyushevsky and Plechov, 2011). Following the guideline for melt inclusion studies (Rose-Koga et al., 2021), we specify that in Petrolog we used the olivine model of Ford et al. (1983), as well as the density model of Lange and Carmichael (1987). The initial oxidation state model used is the model of Kress and Carmichael (1988), and we fixed $Fe^{3+}/(Fe^{2+}+Fe^{3+})$ at 0.2 as determined for the Stromboli lavas (Metrich and
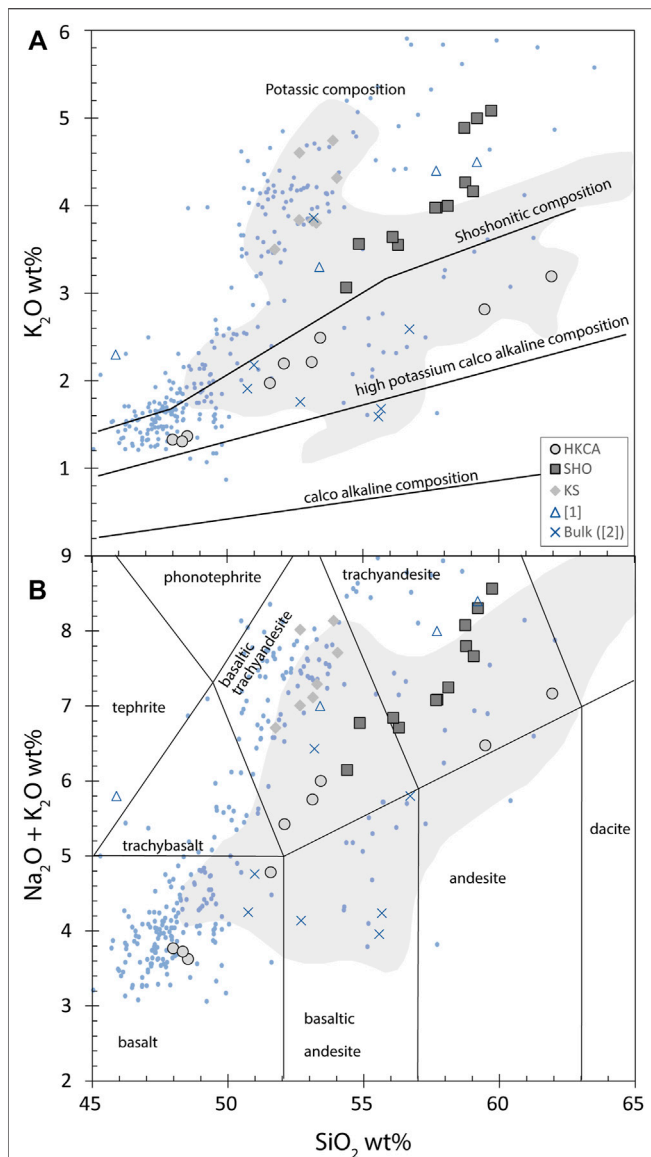
FIGURE 4 | Silica content plotted against **(A)** potassium content and **(B)** $K_2O + Na_2O$ (wt%) for ST2 melt inclusions. Manzini et al. (2017) data from ST2 are also plotted for comparison (empty triangles, [1]), as well as the Stromboli bulk data for which δ37Cl have been calculated ([2]; Liotta et al., 2017; crosses). The shaded field represents whole rocks (georock database) and blue dots ([3]) represent melt inclusions from other Stromboli samples (e.g., Métrich et al., 2001; Bertagnini et al., 2003; Métrich et al., 2010; Rose-Koga et al., 2012; Schiavi et al., 2012). Major elements of melt inclusions entrapped in olivine have been corrected for post-entrapment crystallization.

FIGURE 5 | **(A)** Chlorine and **(B)** sulfur contents compared to K_2O wt% in ST2 melt inclusions. Symbols are the same as in **Figure 4**. **(A)** No relationship between Cl and K_2O is observed. Potassic melt inclusions have lower Cl content than shoshonitic and high potassium calco alkaline ones. All melt inclusions have higher Cl content than bulk rocks. **(B)** High potassium calco alkaline melt inclusions have higher S content than shoshonitic and potassic melt inclusions, which have lost S due to degassing. High potassium calco alkaline melt inclusions have moderate S content compared to Stromboli melt inclusions from the literature, having up to 2,600 µg/g S.

Clocchiatti, 1996). Melt inclusions displayed a large range of major element compositions, with SiO_2 ranging from 48.3 to 62.0 wt% and K_2O from 1.3 to 5.0 wt% (**Figure 4A**), with no systematics between olivine-hosted and pyroxene-hosted melt inclusions. In a TAS diagram (Le Bas et al., 1986), the melt inclusions show broad compositions ranging from basalt to trachyandesite ($Na_2O + K_2O$ ~3.6–8.6 wt%, **Figure 4B**). Major element concentrations generally show similar compositions to bulk rocks (shaded field) with a few points at less evolved values
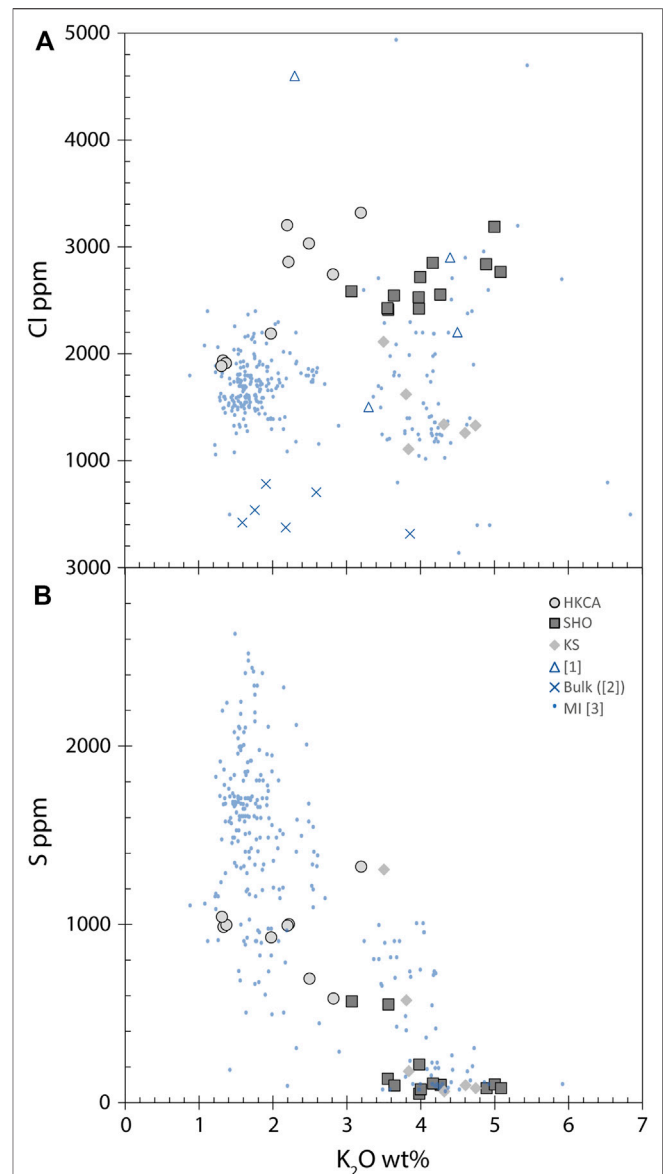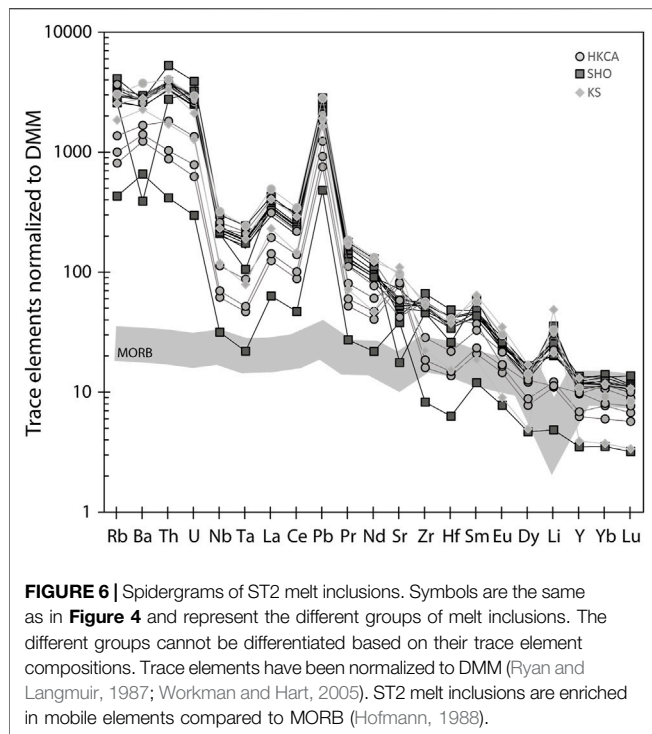
(SiO_2 <50 wt% and $Na_2O + K_2O$ < 4 wt%) corresponding to Fo > 80 olivines. The major element compositions of the melt inclusions are comparable to other melt inclusion studies on Vancori deposits (e.g., Rose-Koga et al., 2012; Manzini et al., 2017), and also comparable to melt inclusion compositions of Stromboli in general (Métrich et al., 2001; Bertagnini et al., 2003; Vaggelli et al., 2003; Schiano et al., 2004; Aiuppa et al., 2010; Métrich et al., 2010).

FIGURE 6 | Spidergrams of ST2 melt inclusions. Symbols are the same as in **Figure 4** and represent the different groups of melt inclusions. The different groups cannot be differentiated based on their trace element compositions. Trace elements have been normalized to DMM (Ryan and Langmuir, 1987; Workman and Hart, 2005). ST2 melt inclusions are enriched in mobile elements compared to MORB (Hofmann, 1988).

Chlorine varies from 1,108 to 3,320 µg/g over the entire range of K_2O (from 1 to 5 wt%) without any significant trend (**Figure 5A**). In contrast, a clear negative correlation exists between S (varying between 49.7 and 1,324 µg/g) and K_2O (**Figure 5B**). The measured matrix glass shows lower Cl concentration (1,199 µg/g) than in the melt inclusions and lower S concentrations (77 µg/g). The highest S content measured in ST2 melt inclusions (1,324 µg/g) is lower than the highest S content reported for Stromboli melt inclusions (up to 2,620 µg/g; Bertagnini et al., 2003). Although H_2O was not measured, we can infer that H_2O concentration in our melt inclusions is low since the total of the major element oxides reaches 100% in many cases (**Supplementary Material S3**). Values from the literature for the amount of H_2O dissolved in Stromboli magma are ~2.7–3.5 wt% prior to outgassing, especially for the present day LP melts, coming from a deep reservoir (Métrich et al., 2010). Therefore, in this study most of the H_2O must have been lost from the melt inclusions (e.g., by H^+ diffusion; Gaetani et al., 2012) or by degassing, as for the present day HP melts (Métrich et al., 2010).

Trace element patterns display the typical features of arc settings, with higher ratios of fluid-mobile elements (B, Pb, U, and LILE) to less fluid-mobile elements (REE, Th, HFSE) than those in MORB (**Figure 6**). Chlorine isotopes range from −2.6 ± 0.1‰ (2 s.e.) to +1.3 ± 0.2‰ (2 s.e.). This range reproduces and extends the range of the five Stromboli values in Manzini et al. (2017), which came from the same sample as that used here. The $\delta^{37}Cl$ weighted average of all melt inclusions from this study and the four melt inclusions from ST2 from Manzini et al. (2017) is −1.15‰, lower than the $\delta^{37}Cl$ weighted average of the bulk rock values

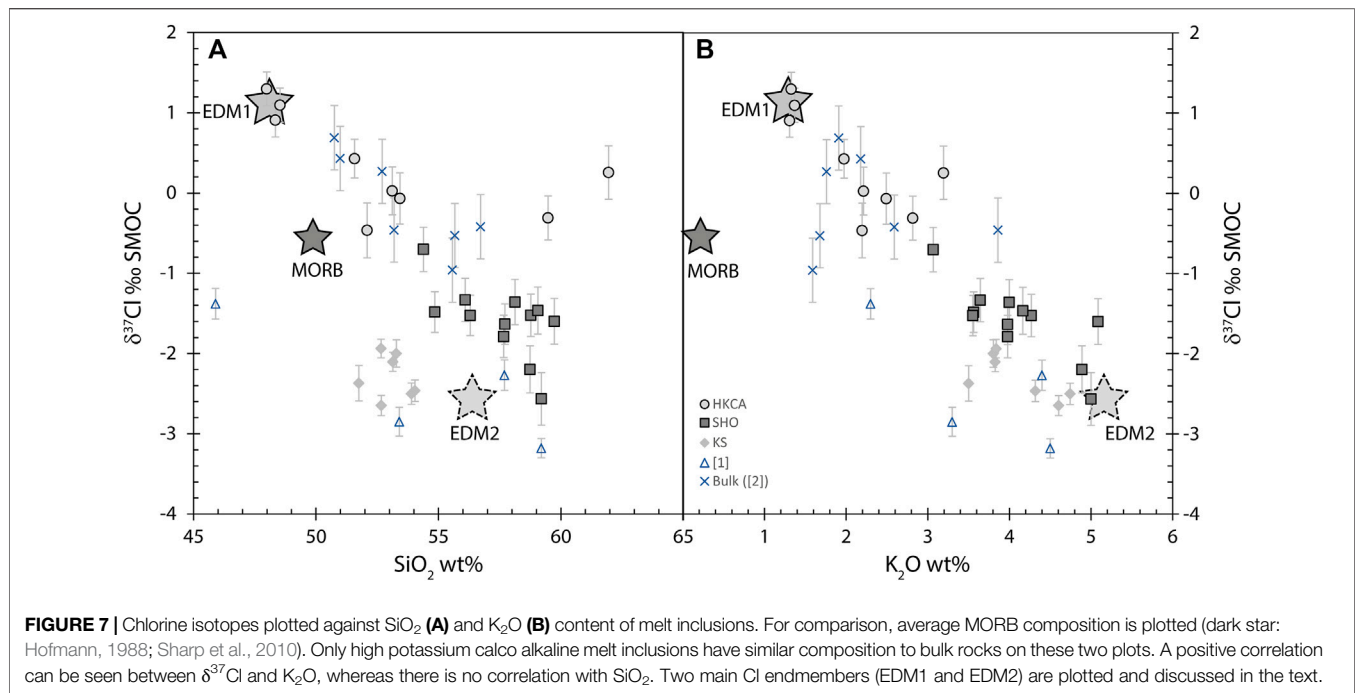(0‰) from Liotta et al. (2017). All results can be found in **Supplementary Material S3**.

DISCUSSION

Chlorine Isotope Variation of Melt Inclusions and Magma Evolution

The 27 melt inclusions and the matrix glass from ST2 studied here span a very large range of major elements, almost as large as the range of erupted lavas on Stromboli (e.g., review from Bertagnini et al., 2008). The melt inclusions can be divided into three groups based on their SiO_2 and K_2O contents, which correspond to the different series shown by the lavas erupted at Stromboli (Peccerillo and Taylor, 1976; Francalanci et al., 2013): high-potassium calco alkaline, shoshonitic, and potassic (**Figure 4**). The olivine hosts of high-potassium calco alkaline melt inclusions have the widest range of Fo content and extend toward the highest Fo content (66.9–84.6, average: 77.5) compared to olivine hosts of potassic and shoshonitic melt inclusions (Fo: 71.5–73.2, average: 72.0, and 66.8–79.0: average: 69.6, respectively). However, there is no clear relationship between the SiO_2 (or K_2O) of the melt inclusions and the Fo content of the host olivine. This suggests that the analyzed crystals from the three series might have formed in different reservoirs, at different stages of their magmatic evolution. The presence of at least three different reservoirs, located at different depths within Stromboli's plumbing system has already been proposed, based on the Sr isotope analysis of whole rock and plagioclases, and on *in situ* geochemical analysis of these plagioclases (Francalanci et al., 2005). One of the reservoirs is sited at a depth of ~10–11 km (e.g., Bertagnini et al., 2003; Pino et al., 2011) and contains a small amount of phenocrysts (generating LP pumices), an intermediate reservoir consists of an old cumulate mush, and the third reservoir, possibly at 1–3 km (e.g., Burton et al., 2007), in which the HP melts originate, is enriched in phenocrysts.

The lack of correlation between Cl and K_2O (**Figure 5A**) suggests different sources of Cl for this sample, given that both are incompatible elements during crystallization and should thus show a positive correlation if derived from a single source. There is no correlation between SiO_2 and $\delta^{37}Cl$ (**Figure 7A**), but no significant $\delta^{37}Cl$ variation within each series was expected as Cl isotopes do not fractionate at magmatic temperatures in the absence of kinetic diffusion (Schauble et al., 2003; Fortin et al., 2017). However, a clear negative correlation between $\delta^{37}Cl$ and K_2O content is observed in the melt inclusions (**Figure 7B**). The correlation cannot be related to analytical bias, despite K_2O being a component of the SIMS data reduction (**Figure 3**). Indeed, UNIL-B4, one of the glass reference materials used for the calibration, has a major element composition very close to those of the Stromboli melt inclusions, especially the shoshonitic and KS melt inclusions, with 56 wt% SiO_2 and 4.34 wt% K_2O (Manzini et al., 2017). Instead, the difference in $\delta^{37}Cl$ between the high-potassium calco alkaline and shoshonitic-potassic melt inclusions is inferred to reflect different Cl sources of the mantle. Two endmembers (EDM1 and EDM2) can be
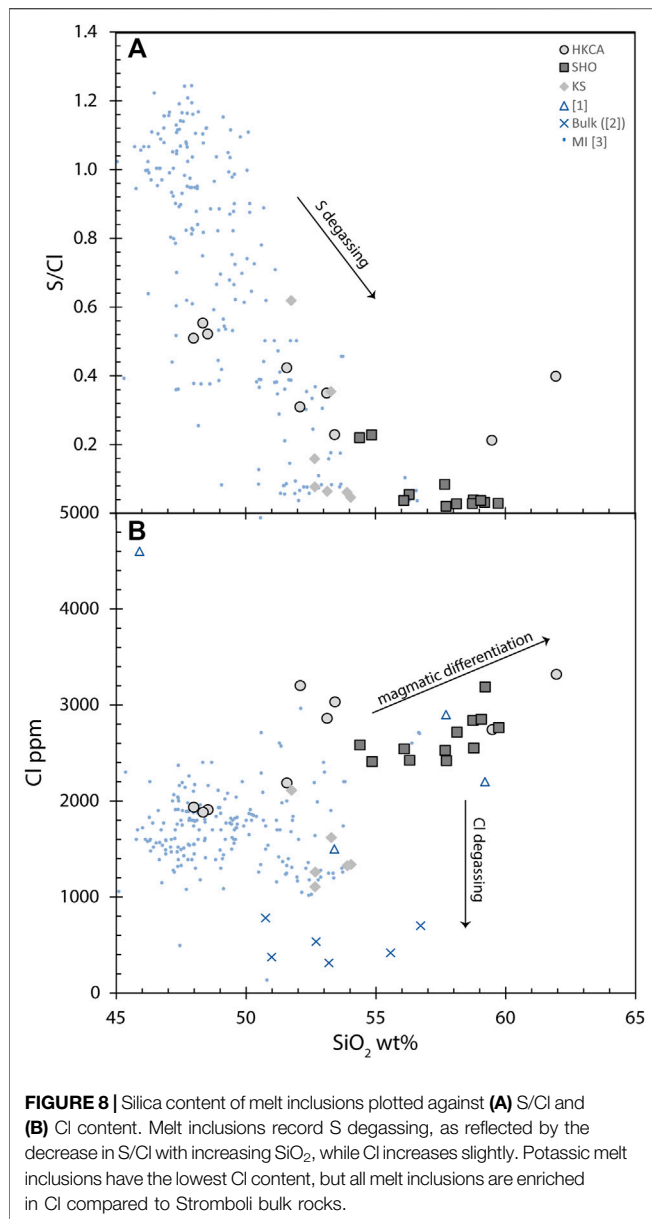
FIGURE 7 | Chlorine isotopes plotted against SiO_2 **(A)** and K_2O **(B)** content of melt inclusions. For comparison, average MORB composition is plotted (dark star: Hofmann, 1988; Sharp et al., 2010). Only high potassium calco alkaline melt inclusions have similar composition to bulk rocks on these two plots. A positive correlation can be seen between $δ^{37}Cl$ and K_2O, whereas there is no correlation with SiO_2. Two main Cl endmembers (EDM1 and EDM2) are plotted and discussed in the text.

identified: EDM1 with high $δ^{37}Cl$ and low K_2O, and EDM2 with low $δ^{37}Cl$ and high K_2O (**Figure 7B**). The nature and origin of these endmembers are discussed in the last section of the discussion.

Influence of Magma Degassing on Chlorine Isotope Composition of Melt Inclusions

In this study, the decrease in S/Cl with increasing K_2O is mainly due to a combination of S degassing and to the increase in Cl concentration (**Figures 5, 8**). Sulfur solubility in basalts is a function of the relative proportions of sulfate and sulfide dissolved in the melt (e.g., Carroll and Webster, 1994; Baker and Moretti, 2011). In addition, S partitions preferentially into the vapor phase (e.g., Scaillet and Pichavant, 2005), whereas Cl is more soluble in melt and is incompatible in anhydrous minerals (e.g., Webster and De Vivo, 2002; Joachim et al., 2017). This results in a progressive increase in Cl during magmatic differentiation, which is observed in melt inclusions from high potassium calco alkaline and shoshonitic (**Figure 8B**). There is no clear trend for the potassic series due to the small number of melt inclusions analyzed (**Figure 8**). We can distinguish melt inclusions in the shoshonitic series which have low S/Cl and $K_2O > 3wt\%$, from melt inclusions in the high potassium calco alkaline series which have slightly higher S/Cl and low $K_2O < 3wt$%. The low S/Cl, high K_2O group has been interpreted as resulting from more extensive exsolution of S at deeper depth than Cl ($≈150$ MPa for S; Spilliaert et al., 2006), associated with a slower rate of magma rise in the case of Etna melt inclusions (Spilliaert et al., 2006). For Stromboli it has been proposed that it results from the redox change of sulfur in the shoshonitic melt (Métrich et al., 2010).

High potassium calco alkaline melt inclusions are the least degassed in terms of S (**Figure 8A**) but are degassed with respect to H_2O based on the totals of the electron probe measurements. However, H_2O loss occurs at a shallower depth than S degassing (Spilliaert et al., 2006) so melt inclusions from high potassium calco alkaline could still represent deeper melts. In terms of Cl content, potassic melt inclusions are the most depleted (**Figure 8B**) but are richer than the bulk rocks. The similar SiO_2 content and lower Cl content of potassic melt inclusions relative to high potassium calco alkaline melt inclusions (**Figure 8B**) could suggest that the potassic melt inclusions are degassed products of high potassium calco alkaline melts. However, the relationship between $δ^{37}Cl$ and K_2O (**Figure 7B**) suggests that there might be two different sources of Cl for these two series.

Based on theoretical fractionation factors, at 600°C, 90% removal of Cl due to HCl degassing would only lower the $δ^{37}Cl$ in the melt by only 0.5‰ (Schauble et al., 2003; Ranta et al., 2021). Since $δ^{37}Cl$ is almost unaffected by equilibrium degassing (e.g., Sharp et al., 2010), there should be no correlation between $δ^{37}Cl$ and Cl content. Similarly, Cl isotopic fractionation between melt and NaCl, RbCl, or KCl gases or liquids is expected to be smaller than for HCl (Schauble et al., 2003; Sharp et al., 2010). However, in the case of Cl kinetic fractionation during degassing (or, more generally, Cl removal from the melt by CO_2 fluxing or during brine formation), ^{35}Cl moves faster, leading to a degassed melt with higher $δ^{37}Cl$ relative to an undegassed melt. Shoshonitic and potassic melt inclusions do not show any relationship between Cl and $δ^{37}Cl$ (**Figure 9A**), whereas there is a slight negative relationship for high potassium calco alkaline melt inclusions, which may represent Cl isotopic fractionation by kinetic diffusion during degassing (or Cl removal). Since potassic

FIGURE 8 | Silica content of melt inclusions plotted against **(A)** S/Cl and **(B)** Cl content. Melt inclusions record S degassing, as reflected by the decrease in S/Cl with increasing SiO2, while Cl increases slightly. Potassic melt inclusions have the lowest Cl content, but all melt inclusions are enriched in Cl compared to Stromboli bulk rocks.

melt inclusions have lower contents of both $\delta^{37}Cl$ and Cl, this is another argument against potassic melts being degassed from high potassium calco alkaline melts and reinforces the hypothesis that there are two different sources of Cl for the two series.

The potential effect of degassing on the Cl isotope values of bulk rocks, as suggested by Manzini et al. (2017), can be indirectly investigated by comparing the $\delta^{37}Cl$ of melt inclusions from ST2 and those of bulk samples from different locations in Stromboli. Almost half of the melt inclusion data has lower $\delta^{37}Cl$ than those of the bulk rocks (**Figure 9A**). Interestingly, high potassium calco alkaline melt inclusions have similar $\delta^{37}Cl$ and major elements to the bulk rocks (**Figures 4**, **7**), which would indicate that no isotopic fractionation had taken place during magmatic degassing of this melt batch. On the contrary, shoshonitic and potassic melt inclusions have lower $\delta^{37}Cl$ compared to the bulk rock $\delta^{37}Cl$

(**Figures 7**, **9A**). Only one bulk rock has similar major elements to the potassic melt inclusions, with a $\delta^{37}Cl$ of $-0.5 \pm 0.4‰$ (Liotta et al., 2017; **Figure 4**), which is statistically higher than the $\delta^{37}Cl$ range for potassic melt inclusions (-1.9 to $-2.6 \pm 0.2‰$). This difference could theoretically be explained by kinetic fractionation during degassing. In that case, potassic melt inclusions, which have lower Cl content, should have a smaller difference from the bulk rocks compared to shoshonitic melt inclusions, as the parental melts of these melt inclusions would suffer a larger Cl loss. Indeed, the greater the Cl loss, the greater the $\delta^{37}Cl$ difference between the bulk rock and melt inclusions in the event of kinematic Cl isotope fractionation. In fact, potassic melt inclusions have a slightly bigger difference with respect to the $\delta^{37}Cl$ bulk rock compared to shoshonitic melt inclusions. A comparison between $\delta^{37}Cl$ and S/Cl (**Figure 9B**), recording S degassing, shows that ST2 melt inclusions demonstrate a positive relationship between these two geochemical indicators. However, S degassing alone should not fractionate $\delta^{37}Cl$. Even if this were to be the case, it would result in an increase in $\delta^{37}Cl$ with decreasing S/Cl due to faster ^{35}Cl diffusion (Fortin et al., 2017), whereas in fact the opposite is observed for ST2 melt inclusions. Therefore, these different observations do not support Cl kinetic fractionation during degassing to explain the differences in $\delta^{37}Cl$ between ST2 melt inclusions, especially those from potassic and shoshonitic series, relative to bulk rock values for Stromboli. The low $\delta^{37}Cl$ in melt inclusions might thus represent a component that is not clearly expressed in the bulk rocks. Indeed, the weighted average $\delta^{37}Cl$ of the melt inclusions ($-1.15‰$), which should represent the bulk $\delta^{37}Cl$ of the ST2 sample, is lower than the average of the seven bulk rock values (Liotta et al., 2017), but is similar to that of the lowest bulk rock value ($-1.0 \pm 0.4‰$). Remarkably, Liotta et al. (2017) also observed a positive relationship between S/Cl and $\delta^{37}Cl$ in Stromboli gases, related to the volcanic activity.

Magma Sources of Chlorine Beneath Stromboli

The correlation between $\delta^{37}Cl$ and K_2O, as well as with S/Cl, in ST2 melt inclusions (**Figures 7B**, **9B**) are most likely due to mixing between two endmembers. We define two possible Cl endmembers: EDM1 with a higher $\delta^{37}Cl$ ($~+1.2‰$), lower K_2O ($~1wt\%$), and higher S/Cl ($~0.6$), and EDM2 with a low $\delta^{37}Cl$ $~$ $-2.6‰$, high K_2O $~5wt\%$, and low S/Cl < 0.1. These endmembers do not have a specific SiO_2 content (**Figure 7A**), with EDM2, represented by the potassic and shoshonitic melt inclusions, having a variable SiO_2 (from 51 to 60 wt%). This means that a primitive melt batch with an imprint of EDM1 or EDM2 will conserve its $\delta^{37}Cl$ signature during magmatic differentiation and degassing.

Chlorine sources are investigated using Cl isotopes combined with trace element ratios. For example, the Ba/La ratio is a tracer of aqueous fluids, as Ba is a fluid-mobile element and La is a fluid-immobile element. Similarly, the La/Yb ratio traces variations in the degree of melting and, more importantly, the possible input of a melt or supercritical liquid component to the mantle source, as both La and Yb are fluid-immobile elements. On a plot of Ba/La against $\delta^{37}Cl$ (**Figure 10A**), melt inclusions display a slight positive
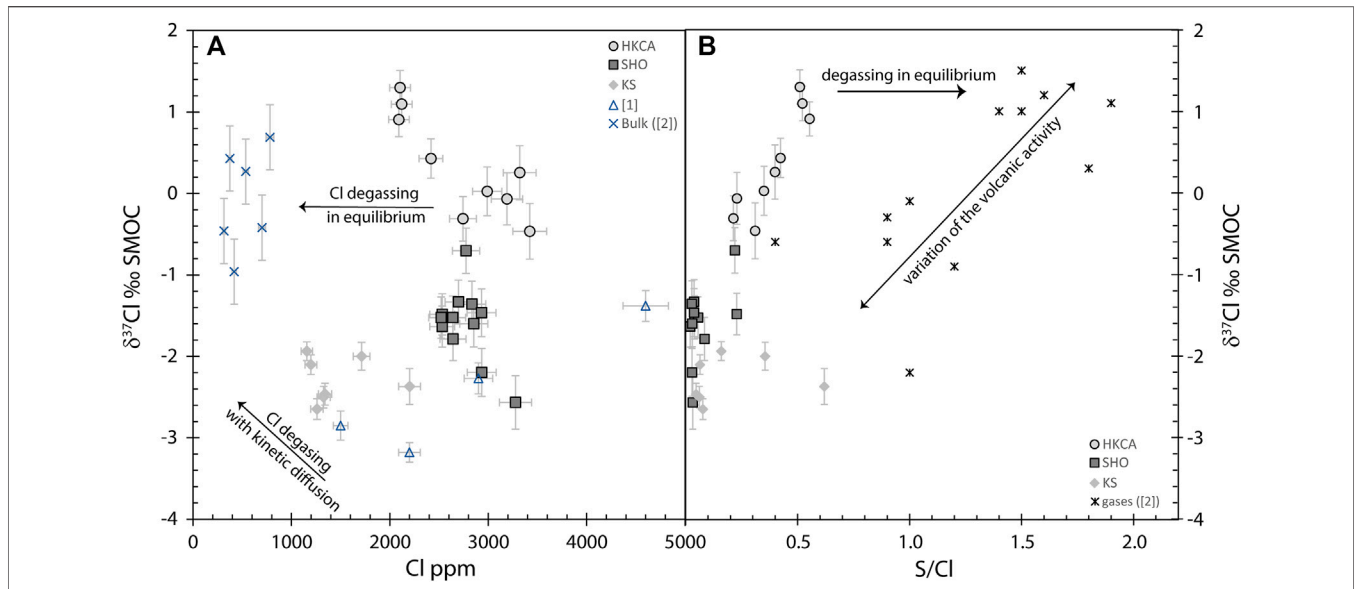
FIGURE 9 | Chlorine isotopes compared to **(A)** Cl content in melt inclusions and **(B)** S/Cl in melt inclusions and gases ([2]: Liotta et al., 2017). **(A)** For comparison, bulk rocks from Stromboli ([2]: Liotta et al., 2017) are plotted, as well as the olivine-hosted melt inclusions from [1]: Manzini et al. (2017). Melt inclusions are all enriched in Cl compared to bulk rocks. Overall, no relationship between Cl and δ37Cl can be seen. **(B)** Melt inclusions have similar δ37Cl to Stromboli gases. As for the gases, a positive correlation can be seen between δ37Cl and S/Cl, which cannot be linked to S or Cl degassing.
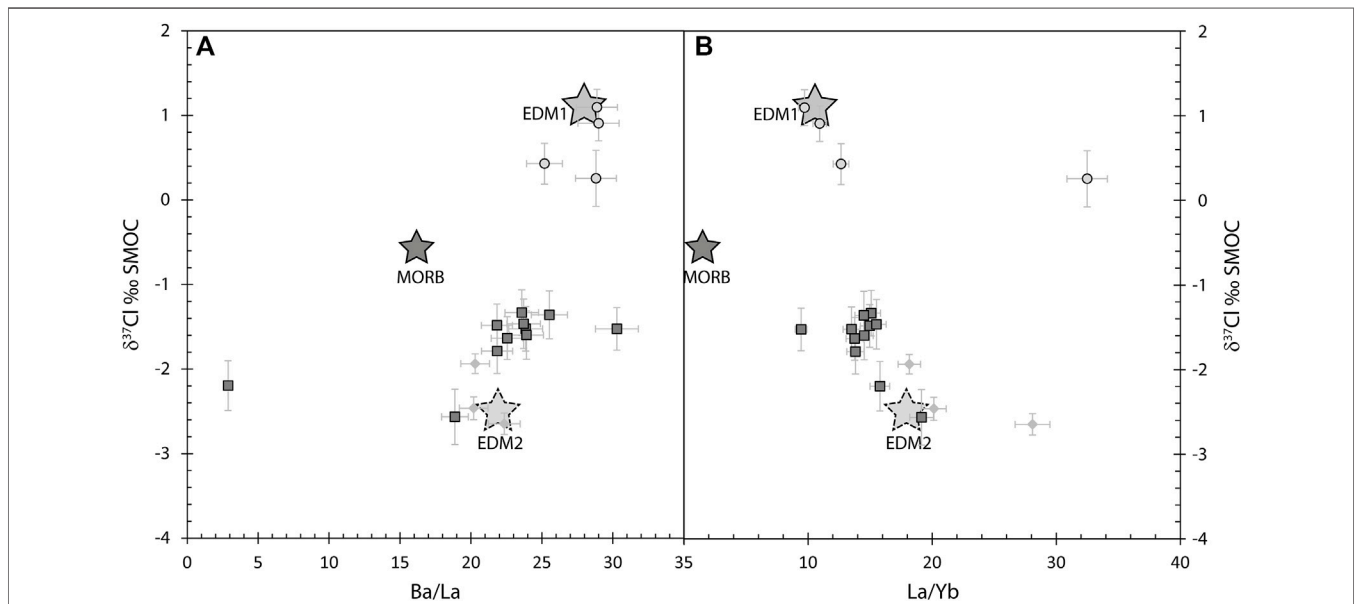
FIGURE 10 | Chlorine isotopes plotted against Ba/La **(A)** and La/Yb **(B)** ratios in melt inclusions. EDM1 and high potassium calco alkaline melt inclusions have higher Ba/La compared to EDM2, shoshonitic, and potassic melt inclusions, whereas EDM2 has a higher La/Yb ratio compared to EDM1. EDM1 is thus more enriched in fluid-mobile elements relative to EDM2.

correlation, with higher Ba/La for EDM1 (~29) compared to EDM2 (~22). Both endmembers have higher Ba/La than MORB (e.g., Hofmann, 1988), reflecting the addition of an aqueous fluid to the mantle wedge, with EDM1 being more enriched in fluid-mobile elements. Similarly, the negative trend between δ37Cl and La/Yb (**Figure 10B**) suggests that the most negative δ37Cl values,

representing EDM2, reflect the influence of a melt-like component or of a supercritical fluid. Their significantly different δ37Cl compositions point strongly to different lithologies.

The positive δ37Cl of EDM1 could reflect the breakdown of amphiboles from the upper slab lithologies. A recent study on electrical conductivity shows amphibole to be one of the principal

hosts of Cl in the slab (Manthilake et al., 2021). Amphibole as residual phase during slab dehydration in low temperature subduction zones has been invoked to explain extremely low Cl and F in melt inclusions (Iwate; Rose-Koga et al., 2014) because it holds on to these halogens and it explains why they are subsequently less abundant in the melt. Here at Stromboli, the steep dip of the Ionian slab (≈70°; e.g., Tommasini et al., 2007), along with the thermal and rheological model, indicates a very cold subduction zone (Carminati et al., 2005; Pasquale et al., 2005). This means that dehydration and melting reactions are possible at greater depths along this slab than in many other volcanic arc systems. So, we hypothesize that in this particular setting, the slab amphibole-bearing lithologies break down and the ensuing fluids that metasomatized the mantle wedge transmit the amphibole δ^{37}Cl signature. Indeed, hydrothermal amphibole veins from oceanic crust have positive values (up to +1.7‰; Barnes and Cisneros, 2012). Melting of amphibole-bearing altered oceanic crust (AOC) has already been invoked to explain the positive δ^{37}Cl values found in the arc lavas from Ecuador (Chiaradia et al., 2014). Also, Pb isotopes on single crystals of amphibole from an arc lava (Guagua Pichincha, Ecuador; Ancellin et al., 2019) showed that the most primitive amphibole had low ^{206}Pb/^{204}Pb, in the order of 18.82–18.88, overlapping with the range of Pb isotopes in the Stromboli melt inclusions (*in situ* measurements:18.76–18.83; Rose-Koga et al., 2012). Therefore, the breakdown of amphibole in amphibole-bearing AOC could pass the identifying features into the fluid agent from the slab that are required to explain the Cl isotope and Pb isotope signatures of Stromboli melt inclusions. EDM1 is represented here by the high potassium calco alkaline melt inclusions (**Figures 7, 10**).

EDM2 has negative δ^{37}Cl values and is represented by the most extreme potassic and shoshonitic melt inclusions. Negative δ^{37}Cl values in arc lavas are usually linked to the influence of seafloor sediment (e.g., Barnes and Sharp, 2017). Thus, the high potassium calco alkaline melt inclusions seem to have recorded the strongest influence of the aqueous fluid originating from the subducting crust whereas the shoshonitic and potassic melt inclusions record the signature of a fluid issued from the subducted sediments enriched in immobile elements. This is in full agreement with Tommasini et al. (2007), who proposed the involvement of an aqueous fluid from the subducting crust and a supercritical liquid from the subducted sediments ± crust for the magma genesis of Stromboli magmas, based on the trace elements and radiogenic isotopes (U, Th, Sr, Nd, Pb) of the whole rocks.

Melt inclusions thus allow two different Cl components from the mantle wedge beneath Stromboli to be highlighted, with each component most probably also playing a role in the different major element signatures of the magmas, as the alkali enrichment of shoshonitic and potassic melts could be related to the addition of fluid derived from sediments. The two Cl components were not discernible in the bulk rock contents, probably due to mixing of different melt batches at a shallow depth prior to eruption, which would have smoothed and averaged the δ^{37}Cl signal. As the gases have a similar range of δ^{37}Cl to the melt inclusions, and a similar relationship for S/Cl (**Figure 9B**), it is possible that the gases at Stromboli actually reflect the degassing of different melt pockets/compositions.

CONCLUSION

The new melt inclusion data from a single hand sample (ST2) span a large range of major element compositions. Based on their major elements, three series are identified, which correspond to three series found in the Stromboli lavas (high potassium calco alkaline, shoshonitic, and potassic). Chlorine isotopes extend the previous melt inclusion data for Stromboli toward more positive values. The δ^{37}Cl vary from −2.6 to +1.2‰, with an average slightly lower than that of the bulk rocks from Stromboli. This large isotopic variation cannot be related to degassing or fractional crystallization. Instead, correlation with K_2O and S/Cl suggest mixing between at least two different sources of Cl. Correlation between δ^{37}Cl and trace elements points toward a first endmember, enriched in fluid mobile elements and with positive δ^{37}Cl, reflecting amphibole breakdown from the AOC. A second endmember, enriched in fluid immobile elements and with negative δ^{37}Cl, records the influence of subducted sediment melts (or supercritical fluids). These Cl sources have different influences on the melt inclusions from the three series: high potassium calco alkaline melt inclusions are most influenced by the aqueous fluid, whereas shoshonitic and potassic melt inclusions have stronger sediment melt signatures. δ^{37}Cl could be a promising tracer for amphibole in the slab fluxes, and could also be a valuable tool to track the role of amphibole in the context of arc magma genesis and differentiation (e.g., Médard et al., 2006; Davidson et al., 2007).

DATA AVAILABILITY STATEMENT

The original contributions presented in the study are included in the article/**Supplementary Material**, further inquiries can be directed to the corresponding author.

AUTHOR CONTRIBUTIONS

A-SB designed the study and did the SIMS measurements, data reduction, and writing. ER-K did sample preparation, LA-ICP-MS measurements, data reduction, and writing. AC prepared the samples, did EMPA measurements, and created some of the figures.

FUNDING

ACKNOWLEDGMENTS

sessions. Thank you to Fran Van Wyk de Vries for proofreading the final version as well as thorough corrections. We are also grateful for the constructive review of RM, the comments of IEMS, and the manuscript handling by the editor HM.

SUPPLEMENTARY MATERIAL

The Supplementary Material for this article can be found online at: https://www.frontiersin.org/articles/10.3389/feart.2021.793259/full#supplementary-material

REFERENCES

Aiuppa, A., Baker, D. R., and Webster, J. D. (2009). Halogens in Volcanic Systems. *Chem. Geology.* 263, 1–18. doi:10.1016/j.chemgeo.2008.10.005

Aiuppa, A., Bertagnini, A., Métrich, N., Moretti, R., Di Muro, A., Liuzzo, M., et al. (2010). A Model of Degassing for Stromboli Volcano. *Earth Planet. Sci. Lett.* 295, 195–204. doi:10.1016/J.EPSL.2010.03.040

Ancellin, M. A., Vlastélic, I., Samaniego, P., Nauret, F., Gannoun, A., and Hidalgo, S. (2019). Up to 1% Pb Isotope Disequilibrium between Minerals Hosted in Dacites from the Guagua Pichincha Volcano, Ecuador: Implication for Tracing the Source and Crustal History of continental Arc Magmas. *Chem. Geol.* 525, 177–189. doi:10.1016/J.CHEMGEO.2019.07.016

Baker, D. R., and Moretti, R. (2011). Modeling the Solubility of Sulfur in Magmas: A 50-Year Old Geochemical Challenge. *Rev. Mineralogy Geochem.* 73, 167–213. doi:10.2138/rmg.2011.73.7

Barberi, F., Innocenti, F., Ferrara, G., Keller, J., and Villari, L. (1974). Evolution of Eolian Arc Volcanism (Southern Tyrrhenian Sea). *Earth Planet. Sci. Lett.* 21, 269–276. doi:10.1016/0012-821X(74)90161-7

Barnes, J. D., and Sharp, Z. D. (2017). Chlorine Isotope Geochemistry. *Rev. Mineralogy Geochem.* 82, 345–378. doi:10.2138/rmg.2017.82.9

Barnes, J. D., Sharp, Z. D., Fischer, T. P., Hilton, D. R., and Carr, M. J. (2009). Chlorine Isotope Variations along the Central American Volcanic Front and Back Arc. *Geochemistry, Geophys. Geosystems* 10 , 1–17. doi:10.1029/2009gc002587

Barnes, J. D., and Cisneros, M. (2012). Mineralogical Control on the Chlorine Isotope Composition of Altered Oceanic Crust. *Chem. Geology.* 326-327, 51–60. doi:10.1016/j.chemgeo.2012.07.022

Barnes, J. D., Sharp, Z. D., and Fischer, T. P. (2008). Chlorine Isotope Variations across the Izu-Bonin-Mariana Arc. *Geol* 36, 883–886. doi:10.1130/G25182A.1

Bertagnini, A., Métrich, N., Francalanci, L., Landi, P., Tommasini, S., and Conticelli, S. (2008). "Volcanology and Magma Geochemistry of the Present-Day Activity: Constraints on the Feeding System," in *The Stromboli Volcano, an Integrated Study of the 2002–2003 Eruption. AGU Geophys*. Editors S. Calvari, S. Inguaggiato, M. Ripepe, and M. Rosi (Washington, DC: Monograph. Series), 19–38.

Bertagnini, A., Métrich, N., Landi, P., and Rosi, M. (2003). Stromboli Volcano (Aeolian Archipelago, Italy): An Open Window on the Deep-Feeding System of a Steady State Basaltic Volcano. *J. Geophys. Res.* 108, 2336. doi:10.1029/2002JB002146

Bouvier, A.-S., Manzini, M., Rose-Koga, E. F., Nichols, A. R. L., and Baumgartner, L. P. (2019). Tracing of Cl Input into the Sub-arc Mantle through the Combined Analysis of B, O and Cl Isotopes in Melt Inclusions. *Earth Planet. Sci. Lett.* 507, 30–39. doi:10.1016/j.epsl.2018.11.036

Bouvier, A., Portnyagin, M. V., Flemetakis, S., Hoernle, K., Klemme, S., Berndt, J., et al. (accepted). Chlorine Isotope Behavior in Subduction Zone Settings Revealed by Olivine-Hosted Melt Inclusions from the Central America Volcanic Arc. *Earth Planet. Sci. Lett.*

B. Scaillet, B., and M. Pichavant, M. (2005). A Model of sulphur Solubility for Hydrous Mafic Melts: Application to the Determination of Magmatic Fluid Compositions of Italian Volcanoes. *Ann. Geophys.* 48 , 671–698. doi:10.4401/ag-3226

Burton, M., Allard, P., Mure´, F., and La Spina, A. (2007). Magmatic Gas Composition Reveals the Source Depth of Slug-Driven Strombolian Explosive Activity. *Science* 317, 227–230. doi:10.1126/SCIENCE.1141900

Carminati, E., Negredo, A. M., Valera, J. L., and Doglioni, C. (2005). Subduction-related Intermediate-Depth and Deep Seismicity in Italy: Insights from thermal and Rheological Modelling. *Phys. Earth Planet. Interiors* 149, 65–79. doi:10.1016/j.pepi.2004.04.006

Carroll, M. R., and Webster, J. D. (1994). *Sulfur, Noble Gases, and Halogens: Solubility Relations of the Less Abundant Volatile Species in Magmas*. Reviews in Mineralogy, V30. United States: Mineralogical Society of America, 331–371.

Chiaradia, M., Barnes, J. D., and Cadet-Voisin, S. (2014). Chlorine Stable Isotope Variations across the Quaternary Volcanic Arc of Ecuador. *Earth Planet. Sci. Lett.* 396, 22–33. doi:10.1016/j.epsl.2014.03.062

Cisneros, M. (2013). *An Experimental Calibration of Chlorine Isotope Fractionation between Amphibole and Fluid at 700 °C and 0.2 GPa*. Austin, TX: The University of Texas at Austin.

Danyushevsky, L. V., and Plechov, P. (2011). Petrolog3: Integrated Software for Modeling Crystallization Processes. *Geochem. Geophys. Geosyst.* 12 , 1–32. doi:10.1029/2011GC003516

Davidson, J., Turner, S., Handley, H., Macpherson, C., and Dosseto, A. (2007). Amphibole "Sponge" in Arc Crust? *Geol* 35, 787. doi:10.1130/G23637A.1

De Astis, G., Peccerillo, A., Kempton, P. D., La Volpe, L., Wu, T. W., and Orabona, V. (2000). Transition from Calc-Alkaline to Potassium-Rich Magmatism in Subduction Environments: Geochemical and Sr, Nd, Pb Isotopic Constraints from the Island of Vulcano (Aeolian Arc). *Contrib. Mineralogy Petrol.* 139, 684–703. doi:10.1007/s004100000172

Ellam, R. M., and Harmon, R. S. (1990). Oxygen Isotope Constraints on the Crustal Contribution to the Subduction-Related Magmatism of the Aeolian Islands, Southern Italy, *J. Volcanology Geothermal Res.* 44, 105–122. doi:10.1016/0377-0273(90)90014-7

Ellam, R. M., Hawkesworth, C. J., Menzies, M. A., and Rogers, N. W. (1989). The Volcanism of Southern Italy: Role of Subduction and the Relationship between Potassic and Sodic Alkaline Magmatism. *J. Geophys. Res.* 94, 4589–4601. doi:10.1029/JB094IB04P04589

Ford, C. E., Russell, D. G., Craven, J. A., and Fisk, M. R. (1983). Olivine-Liquid Equilibria: Temperature, Pressure and Composition Dependence of the Crystal/Liquid Cation Partition Coefficients for Mg, Fe2+, Ca and Mn. *J. Petrol.* 24, 256–266. doi:10.1093/PETROLOGY/24.3.256

Fortin, M.-A., Watson, E. B., and Stern, R. (2017). The Isotope Mass Effect on Chlorine Diffusion in Dacite Melt, with Implications for Fractionation during Bubble Growth. *Earth Planet. Sci. Lett.* 480, 15–24. doi:10.1016/j.epsl.2017.09.042

Francalanci, L., Avanzinelli, R., Tommasini, S., and Heuman, A. (2007). A West-East Geochemical and Isotopic Traverse along the Volcanism of the Aeolian Island Arc, Southern Tyrrhenian Sea, Italy: Inferences on Mantle Source Processes. *Spec. Pap. Geol. Soc. Am.* 418, 235–263. doi:10.1130/2007.2418(12)

Francalanci, L., Barbieri, M., Manetti, P., Peccerillo, A., and Tolomeo, L. (1988). Sr Isotopic Systematics in Volcanic Rocks from the Island of Stromboli, Italy (Aeolian Arc). *Chem. Geology. Isotope Geosci. section* 73, 109–124. doi:10.1016/0168-9622(88)90010-3

Francalanci, L., Davies, G. R., Lustenhouwer, W., Tommasini, S., Mason, P. R. D., and Conticelli, S. (2005). Intra-Grain Sr Isotope Evidence for Crystal Recycling and Multiple Magma Reservoirs in the Recent Activity of Stromboli Volcano, Southern Italy. *South. Italy. J. Petrol.* 46, 1997–2021. doi:10.1093/petrology/egi045

Francalanci, L., Lucchi, F., Keller, J., De Astis, G., and Tranne, C. A. (2013). Chapter 13 Eruptive, Volcano-Tectonic and Magmatic History of the Stromboli Volcano (north-eastern Aeolian Archipelago). *Geol. Soc. Lond. Mem.* 37, 397–471. doi:10.1144/M37.13

Francalanci, L., Manetti, P., and Peccerillo, A. (1989). Volcanological and Magmatological Evolution of Stromboli Volcano (Aeolian Islands): The Roles of Fractional Crystallization, Magma Mixing, Crustal Contamination and Source Heterogeneity. *Bull. Volcanol.* 51 (51), 355–378. doi:10.1007/BF01056897

Francalanci, L, Taylor, S. R., Mcculloch, M. T., and Woodhead, J. D. (1993). Geochemical and Isotopic Variations in the Calc-Alkaline Rocks of Aeolian

Arc, Southern Tyrrhenian Sea, Italy: Constraints on Magma Genesis. *Contr. Mineral. Petrol.* 113, 300–313. doi:10.1007/bf00286923

Francalanci, L., Tommasini, S., and Conticelli, S. (2004). The Volcanic Activity of Stromboli in the 1906-1998 AD Period: Mineralogical, Geochemical and Isotope Data Relevant to the Understanding of the Plumbing System. *J. Volcanology Geothermal Res.* 131, 179–211. doi:10.1016/S0377-0273(03)00362-7

Gaetani, G. a., O'Leary, J. a., Shimizu, N., Bucholz, C. E., and Newville, M. (2012). Rapid Reequilibration of H2O and Oxygen Fugacity in Olivine-Hosted Melt Inclusions. *Geology* 40, 915–918. doi:10.1130/G32992.1

Gasparini, C., Iannaccone, G., Scandone, P., and Scarpa, R. (1982). Seismotectonics of the Calabrian Arc. *Tectonophysics* 84, 267–286. doi:10.1016/0040-1951(82)90163-9

Godon, A., Webster, J. D., Layne, G. D., and Pineau, F. (2004). Secondary Ion Mass Spectrometry for the Determination of δ37Cl. Part II. Intercalibration of SIMS and IRMS for Aluminosilicate Glasses. *Chem. Geology.* 207, 291–303. doi:10.1016/j.chemgeo.2004.04.003

Gvirtzman, Z., and Nur, A. (2001). Residual Topography, Lithospheric Structure and Sunken Slabs in the central Mediterranean. *Earth Planet. Sci. Lett.* 187, 117–130. doi:10.1016/S0012-821X(01)00272-2

Gvirtzman, Z., and Nur, A. (1999). The Formation of Mount Etna as the Consequence of Slab Rollback. *Nature* 401, 782–785. doi:10.1038/44555

Hofmann, A. W. (1988). Chemical Differentiation of the Earth: the Relationship between Mantle, continental Crust, and Oceanic Crust. *Earth Planet. Sci. Lett.* 90, 297–314. doi:10.1016/0012-821X(88)90132-X

Jambon, A., Déruelle, B., Dreibus, G., and Pineau, F. (1995). Chlorine and Bromine Abundance in MORB: the Contrasting Behaviour of the Mid-Atlantic Ridge and East Pacific Rise and Implications for Chlorine Geodynamic Cycle. *Chem. Geology.* 126, 101–117. doi:10.1016/0009-2541(95)00112-4

Jarosewich, E., Nelen, J. A., and Norberg, J. A. (1980). Reference Samples for Electron Microprobe Analysis. *Geostand. Newsl.* 4, 43–47. doi:10.1111/J.1751-908X.1980.TB00273.X

Joachim, B., Stechern, A., Ludwig, T., Konzett, J., Pawley, A., Ruzié-Hamilton, L., et al. (2017). Effect of Water on the Fluorine and Chlorine Partitioning Behavior between Olivine and Silicate Melt. *Contrib. Mineral. Petrol.* 172, 15. doi:10.1007/s00410-017-1329-1

Kress, V. C., and Carmichael, I. S. E. (1988). Stoichiometry of the Iron Oxidation Reaction in Silicate Melts. *Am. Mineral.* 73, 1267–1274.

Lange, R. A., and Carmichael, I. S. E. (1987). Densities of Na2O-K2o-CaO-MgO-FeO-Fe2O3-Al2O3-TiO2-SiO2 Liquids: New Measurements and Derived Partial Molar Properties. *Geochimica et Cosmochimica Acta* 51, 2931–2946. doi:10.1016/0016-7037(87)90368-1

Layne, G. D., Kent, A. J. R., and Bach, W. (2009). δ37Cl Systematics of a Backarc Spreading System: The Lau Basin. *Geology* 37, 427–430. doi:10.1130/G25520A.1

Le Bas, M. J., Maitre, R. W. L., Streckeisen, A., and Zanettin, B. (1986). A Chemical Classification of Volcanic Rocks Based on the Total Alkali-Silica Diagram. *J. Petrol.* 27, 745–750. doi:10.1093/petrology/27.3.745

Le Voyer, M., Asimow, P. D., Mosenfelder, J. L., Guan, Y., Wallace, P. J., Schiano, P., et al. (2014). Zonation of H2O and F Concentrations Around Melt Inclusions in Olivines. *J. Petrol.* 55, 685–707. doi:10.1093/petrology/egu003

Le Voyer, M., Rose-Koga, E. F., Shimizu, N., Grove, T. L., and Schiano, P. (2010). Two Contrasting H2O-Rich Components in Primary Melt Inclusions from Mount Shasta. *J. Petrol.* 51, 1571–1595. doi:10.1093/petrology/egq030

Liotta, M., Rizzo, A. L., Barnes, J. D., D'Auria, L., Martelli, M., Bobrowski, N., et al. (2017). Chlorine Isotope Composition of Volcanic Rocks and Gases at Stromboli Volcano (Aeolian Islands, Italy): Inferences on Magmatic Degassing Prior to 2014 Eruption. *J. Volcanology Geothermal Res.* 336, 168–178. doi:10.1016/j.jvolgeores.2017.02.018

Manthilake, G., Koga, K. T., Peng, Y., and Mookherjee, M. (2021). Halogen Bearing Amphiboles, Aqueous Fluids, and Melts in Subduction Zones: Insights on Halogen Cycle from Electrical Conductivity. *J. Geophys. Res. Solid Earth* 126, e2020JB021339. doi:10.1029/2020JB021339

Manzini, M., Bouvier, A.-S., Barnes, J. D., Bonifacie, M., Rose-Koga, E. F., Ulmer, P., et al. (2017). SIMS Chlorine Isotope Analyses in Melt Inclusions from Arc Settings. *Chem. Geology.* 449, 112–122. doi:10.1016/j.chemgeo.2016.12.002

Marschall, H. R., Wanless, V. D., Shimizu, N., Pogge von Strandmann, P. A. E., Elliott, T., and Monteleone, B. D. (2017). The boron and Lithium Isotopic

Composition of Mid-ocean ridge Basalts and the Mantle. *Geochimica et Cosmochimica Acta* 207, 102–138. doi:10.1016/j.gca.2017.03.028

Médard, E., Schmidt, M. W., Schiano, P., and Ottolini, L. (2006). Melting of Amphibole-Bearing Wehrlites: An Experimental Study on the Origin of Ultra-calcic Nepheline-Normative Melts. *J. Petrol.* 47, 481–504. doi:10.1093/petrology/egi083

Meletti, C., Patacca, E., and Scandone, P. (2000). Construction of a Seismotectonic Model: The Case of Italy. *Pure Appl. Geophys.* 157, 11–35. doi:10.1007/PL00001089

Métrich, N., Bertagnini, A., and Di Muro, A. (2010). Conditions of Magma Storage, Degassing and Ascent at Stromboli: New Insights into the Volcano Plumbing System with Inferences on the Eruptive Dynamics. *J. Petrol.* 51, 603–626. doi:10.1093/petrology/egp083

Métrich, N., Bertagnini, A., Landi, P., and Rosi, M. (2001). Crystallization Driven by Decompression and Water Loss at Stromboli Volcano (Aeolian Islands, Italy). *J. Petrol.* 42, 1471–1490. doi:10.1093/petrology/42.8.1471

Metrich, N., and Clocchiatti, R. (1996). Sulfur Abundance and its Speciation in Oxidized Alkaline Melts. *Geochimica et Cosmochimica Acta* 60, 4151–4160. doi:10.1016/s0016-7037(96)00229-3

Pasquale, V., Verdoya, M., and Chiozzi, P. (2005). Thermal Structure of the Ionian Slab. *Pure Appl. Geophys.* 162, 967–986. doi:10.1007/s00024-004-2651-x

Peccerillo, A., and Taylor, S. R. (1976). Geochemistry of Eocene Calc-Alkaline Volcanic Rocks from the Kastamonu Area, Northern Turkey. *Contr. Mineral. Petrol.* 58, 63–81. doi:10.1007/BF00384745

Pino, N. A., Moretti, R., Allard, P., and Boschi, E. (2011). Seismic Precursors of a Basaltic Paroxysmal Explosion Track Deep Gas Accumulation and Slug Upraise. *J. Geophys. Res.* 116, 2312. doi:10.1029/2009JB000826

Pontevivo, A., and Panza, G. F. (2006). The Lithosphere-Asthenosphere System in the Calabrian Arc and Surrounding Seas - Southern Italy. *Pure Appl. Geophys.* 163, 1617–1659. doi:10.1007/S00024-006-0093-3

Ranta, E., Halldórsson, S. A., Barnes, J. D., Jónasson, K., and Stefánsson, A. (2021). Chlorine Isotope Ratios Record Magmatic Brine Assimilation during Rhyolite Genesis. *Geochem. Persp. Let.* 16, 35–39. doi:10.7185/GEOCHEMLET.2101

Rose-Koga, E. F., Bouvier, A.-S., Gaetani, G. A., Wallace, P. J., Allison, C. M., Andrys, J. A., et al. (2021). Silicate Melt Inclusions in the New Millennium: A Review of Recommended Practices for Preparation, Analysis, and Data Presentation. *Chem. Geology.* 570, 120145. doi:10.1016/j.chemgeo.2021.120145

Rose-Koga, E. F., Koga, K. T., Hamada, M., Hélouis, T., Whitehouse, M. J., and Shimizu, N. (2014). Volatile (F and Cl) Concentrations in Iwate Olivine-Hosted Melt Inclusions Indicating Low-Temperature Subduction. *Earth, Planets and Space* 66, 81. doi:10.1186/1880-5981-66-81

Rose-Koga, E. F., Koga, K. T., Schiano, P., Le Voyer, M., Shimizu, N., Whitehouse, M. J., et al. (2012). Mantle Source Heterogeneity for South Tyrrhenian Magmas Revealed by Pb Isotopes and Halogen Contents of Olivine-Hosted Melt Inclusions. *Chem. Geology.* 334, 266–279. doi:10.1016/j.chemgeo.2012.10.033

Ryan, J. G., and Langmuir, C. H. (1987). The Systematics of Lithium Abundances in Young Volcanic Rocks. *Geochimica et Cosmochimica Acta* 51, 1727–1741. doi:10.1016/0016-7037(87)90351-6

Schauble, E. A., Rossman, G. R., Taylor, H. P., Taylor, H. P., J., and Taylor, H. P. J. (2003). Theoretical Estimates of Equilibrium Chlorine-Isotope Fractionations. *Geochimica et Cosmochimica Acta* 67, 3267–3281. doi:10.1016/S0016-7037(00)01375-310.1016/s0016-7037(02)01375-3

Schiano, P., Clocchiatti, R., Ottolini, L., and Sbrana, A. (2004). The Relationship between Potassic, Calc-Alkaline and Na-Alkaline Magmatism in South Italy Volcanoes: A Melt Inclusion Approach. *Earth Planet. Sci. Lett.* 220, 121–137. doi:10.1016/S0012-821X(04)00048-2

Schiavi, F., Kobayashi, K., Nakamura, E., Tiepolo, M., and Vannucci, R. (2012). Trace Element and Pb-B-Li Isotope Systematics of Olivine-Hosted Melt Inclusions: Insights into Source Metasomatism beneath Stromboli (Southern Italy). *Contrib. Mineral. Petrol.* 163, 1011–1031. doi:10.1007/s00410-011-0713-5

Sharp, Z. D., Barnes, J. D., Fischer, T. P., and Halick, M. (2010). An Experimental Determination of Chlorine Isotope Fractionation in Acid Systems and Applications to Volcanic Fumaroles. *Geochimica et Cosmochimica Acta* 74, 264–273. doi:10.1016/j.gca.2009.09.032

Spilliaert, N., Metrich, N., and Allard, P. (2006). S-Cl-F Degassing Pattern of Water-Rich Alkali basalt: Modelling and Relationship with Eruption Styles on Mount Etna Volcano. *Earth Planet. Sci. Lett.* 248, 772–786. doi:10.1016/j.epsl. 2006.06.031

Tommasini, S., Heumann, A., Avanzinelli, R., and Francalanci, L. (2007). The Fate of High-Angle Dipping Slabs in the Subduction Factory: an Integrated Trace Element and Radiogenic Isotope (U, Th, Sr, Nd, Pb) Study of Stromboli Volcano, Aeolian Arc, Italy. *J. Petrol.* 48, 2407–2430. doi:10.1093/petrology/ egm066

Vaggelli, G., Francalanci, L., Ruggieri, G., and Testi, S. (20032003). Persistent Polybaric Rests of Calc-Alkaline Magmas at Stromboli Volcano, Italy: Pressure Data from Fluid Inclusions in Restitic Quartzite Nodules. *Bull. Volcanology* 65, 385–404. doi:10.1007/S00445-002-0264-8

Webster, J. D., and De Vivo, B. (2002). Experimental and Modeled Solubilities of Chlorine in Aluminosilicate Melts, Consequences of Magma Evolution, and Implications for Exsolution of Hydrous Chloride Melt at Mt. Somma-Vesuvius. *Am. Mineral.* 87, 1046–1061. doi:10.2138/am-2002-8-902

Workman, R. K., and Hart, S. R. (2005). Major and Trace Element Composition of the Depleted MORB Mantle (DMM). *Earth Planet. Sci. Lett.* 231, 53–72. doi:10. 1016/j.epsl.2004.12.005